Non-linear scanning switch-off microscopy for super-resolution fluorescence imaging

Zhaoshuai Gao
Shanghai Jiao Tong University
Shangguo Hou
Shenzhen Bay Laboratory
Suhui Deng
Nanchang University
Le Liang
Wuhan University
Fei Wang
sjtu https://orcid.org/0000-0003-3948-6899
Linjie Guo
Chinese Academy of Sciences
Weina Fang
Chinese Academy of Sciences
Qian Li
Shanghai Jiao Tong University https://orcid.org/0000-0002-1166-6583
Bin Kang
Nanjing University https://orcid.org/0000-0002-8304-103X
Hong-Yuan Chen
Nangjing University https://orcid.org/0000-0001-5217-668X
Chunhai Fan (fanchunhai@sjtu.edu.cn)
Shanghai Jiao Tong University https://orcid.org/0000-0002-7171-7338

Article

Keywords:

Posted Date: September 7th, 2022

DOI: https://doi.org/10.21203/rs.3.rs-1928236/v1

Non-linear scanning switch-off microscopy for super-resolution fluorescence imaging

Zhaoshuai Gao[1,2,8], Shangguo Hou[3,4,8], Suhui Deng[3,5,8], Le Liang[3,6], Fei Wang[1], Linjie Guo[3,7], Weina Fang[3], Qian Li[1], Bin Kang[2*], Hong-Yuan Chen[2*], Chunhai Fan[1*]

[1] School of Chemistry and Chemical Engineering, Frontiers Science Center for Transformative Molecules and National Center for Translational Medicine, Shanghai Jiao Tong University, 200240 Shanghai, China.
[2] School of Chemistry and Chemical Engineering, State Key Laboratory of Analytical Chemistry for Life Science and Collaborative Innovation Center of Chemistry for Life Sciences, Nanjing University, 210023 Nanjing, China.
[3] CAS Key Laboratory of Interfacial Physics and Technology, Shanghai Institute of Applied Physics, Chinese Academy of Sciences, 201800 Shanghai, China.
[4] Institute of Systems and Physical Biology, Shenzhen Bay Laboratory, 518055 Shenzhen, China.
[5] School of Information Engineering, Nanchang University, 330031 Nanchang, China.
[6] The Institute for Advanced Studies, Wuhan University, 430072 Wuhan, China.
[7] The Interdisciplinary Research Center, Shanghai Synchrotron Radiation Facility, Zhangjiang Laboratory, Shanghai Advanced Research Institute, Chinese Academy of Sciences, 201210 Shanghai, China.
[8] These authors contributed equally: Zhaoshuai Gao, Shangguo Hou, Suhui Deng.

Correspondence should be addressed to: binkang@nju.edu.cn (B.K.), hychen@nju.edu.cn (H.-Y.C.) or fanchunhai@sjtu.edu.cn (C.F.).

Abstract

Super-resolution (SR) microscopy provides a revolutionary approach to study cells and animals by breaking the diffraction limit of optical imaging. However, the popularity of the super-resolution microscope in biological sciences remains to be impeded by the high cost of hardware and/or the complexity of software. Here, we present a conceptually different non-linear scanning switch-off microscopy (nSSM) that exploits the omnipresent switch-off effect of fluorophores to enable super-resolution imaging beyond the diffraction limit. We develop a theoretical model of nSSM and experimentally implement the nSSM scheme with an unmodified confocal microscope. We also release a free code for the automatic reconstruction of super-resolution images. By measuring the PSF of the imaged DNA origami nanostructure and mammalian cytoskeleton structures, we demonstrate an SR resolution of ~100 nm that excels the optical resolution limit by over two folds. We further show the generality of nSSM using a range of commercially available fluorescent dyes and proteins to realize SR imaging in various settings. This nSSM methodology may in principle empower any confocal microscope to implement SR imaging to promote biological research.

Main

During the past decades, super-resolution (SR) microscopy has extended our biological landscape by revealing substantial details of the samples[1, 2]. However, the popularity the super-resolution microscopy remains to be hampered by special instrumentation with complex optical set-up and/or heavy computing burden[3]. This instrument barrier restricts the general use of SR imaging in biological research.

To date, confocal fluorescence microscope with its irreplaceable optical section ability, excellent signal/background ratio and reasonably high resolution, remains to be a major workhorse in most biological and medical laboratories[4, 5]. In principle, developing SR imaging schemes based on regular confocal microscope framework is the most effective way to break this instrument barrier. Sample handling approach, like expansion microscopy[6], special inorganic nanoparticles labelling[7-9], can be used to empower a conventional microscope with super-resolution imaging. Moreover, based on the optical geometry of confocal microscopy, the achieved developments such as image scanning microscopy[10, 11], focal modulation microscopy[12], confocal rescan microscopy[13] has obtained remarkable resolution enhancement with the assistance of the special optical geometry and array detector. Nonetheless, the sample handling approach and the instrument modification approach still rely on complex sample processing process or special optical components and/or special inorganic nanoparticles with low labeling density. These restrictions pose limits on application scenarios.

Super-resolution microscopy is an art of distinguishing. The core of distinguishing is to control the emission state of fluorescent probe within diffraction limit area which is founded on specific photophysical effect[14]. Nonlinear photophysical effect of fluorescent probe plays an important role in the developing of super-resolution microscopy[15]. Different with widefield microscope, the point illumination strategy of confocal microscope supplies high excitation power density which is essential for inducing non-linear effect on fluorescent probe. Meanwhile, as organic dye and fluorescent protein are the most widely used probe in biology study, most of the super-resolution fluorescence microscopy is developed centered on these two types of probe[16, 17].

In this contribution, by exploiting the fluorescence switch-off effect, we developed a conceptual new non-linear scanning switch-off microscopy (nSSM) method for SR imaging on a regular confocal microscope with the standard Gaussian excitation laser scanning spot. Given that SR imaging is an art of distinguishing to control the emission state of fluorophores within the diffraction limit area via nonlinear photophysical effect. Nonlinear tuning the photophysical properties of flurophores has been explored to develop various SR schemes including saturated absorption competition microscopy[18, 19], non-linear structured illumination microscopy[20], nonlinear focal modulation microscopy[12]. Especially, the photon switch-off effects, such as photon bleaching, quenching and reversing, have been popularly employed to tune optical responses of small-molecular fluorescent dyes and fluorescent proteins[15, 21-23]. In our nSSM scheme, under the appropriate exposure dose of the excitation laser, the fluorophore sheds fluorescence only on part of the excitation laser spot of confocal microscope, resulting in a squashed point spread function (PSF). We developed the theoretical framework for

nSSM and experimentally implemented it. We also designed an algorithm to automatically reconstruct SR images. Using a conventional confocal microscope without any instrument modification, we realized ~100 nm resolution that represents a two-fold increase.

Principle and simulation of nSSM. The photoswitchable probe can be reversibly switched between a fluorescent on state with an excitation laser and a nonfluorescent off state with an activated laser[16, 24, 25] (Fig. 1a). In this photophysical process, the fluorescence intensity will increase with the excitation laser increase when the excitation laser is relatively low. However, when the incident light increases to a level at which the switch off process is dominant, the probe will accumulate on dark state

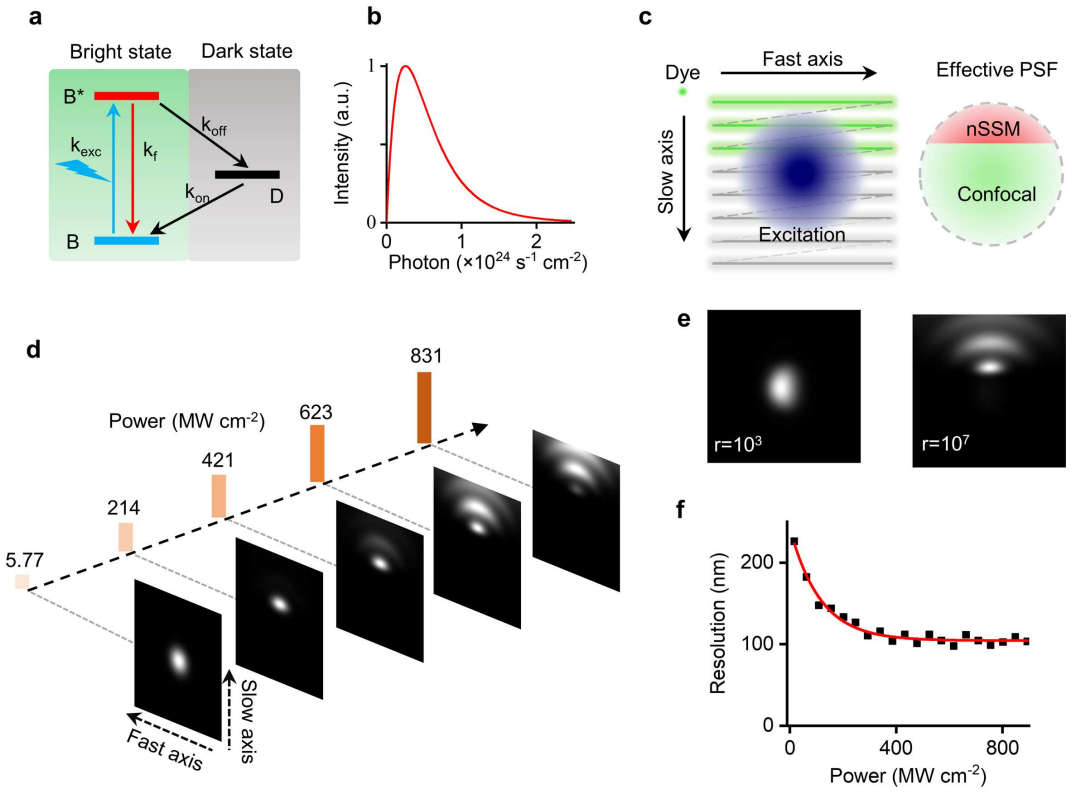

Fig. 1| Principle and simulation of nSSM. a, Simplified energy level diagram with bright state and dark state of a typical switchable fluorophore. **b**, The fluorescence intensity will increase with relative low incident photon flux, whereas it will decrease with relative high incident photon flux. **c,** Scheme of the nSSM principle. For nSSM, the dye walks into the excitation laser spot of the confocal microscope, but only shed fluorescence photon within half of the laser spot. The green and gray line indicate the dye molecule in the on and off state, respectively. The effective PSF of the confocal microscope (green) showed as a circular Gauss shaped PSF, whereas the effective PSF of the nSSM (red) showed as a squashed Gaussian PSF. **d**, The fluorescence intensity response with the increasing excitation laser power. The simulated shaped PSF with cumulative photon flux. **e**, the PSF influenced by r= k_{off}/k_{on}. **f**, Resolution represented by FWHM extracted from the mainlobe of the simulated PSF. Solid red line is fitted curve using R=138exp(-P/114)+104,where P indicate the power of the incident laser.

rapidly. As a result, the fluorescence intensity drops rapidly with the cumulating of the excitation light dose (Fig. 1b). For confocal microscope, as the fluorescence molecule walks into the standard Gaussian excitation laser spot, the fluorescence molecular will take in cumulative exposure dose. That is, under appropriate excitation laser power or dwell time, the fluorophore only sheds fluorescence in part of the excitation laser spot of the confocal microscope, which results in a squashed confocal microscope PSF (Fig. 1c). We reason that the resolution is enhanced in the direction of the scanning slow axis while orthometric-direction scanning enhances the resolution in all directions. Software reconstruction results in the acquired multi-direction SR images.

Physically, based on the transient response of the fluorescence intensity, we model the photon photoswitching process of the fluorescent dye (Fig 1a, Methods). According to our simulation results, with the incident light increase, the shape of the fluorescence PSF turns to ellipse and the sidelobes gradually emerge (Fig. 1d, Supplementary Video). Here, the mainlobe is the effective signal and the sidelobes will deteriorate the imaging performance. In a subsequent image process step, the sidelobes are eliminated. Also, high switching ratio of the probe is a vital property for the realization of nSSM. We define the switching ratio as $r = k_{off}/k_{on}$, in which $r > 10^7$ is essential for nSSM (Fig. 1e, Supplementary Fig. 1). From the calculated nSSM PSF, we quantized the resolution by measuring the full-width at half-maximum (FWHM) of the mainlobe. The resolution is enhanced to ~100 nm with the cumulative exposure laser dose (Fig. 1f).

Image reconstruction algorithm. Following the nSSM work flow, we generated a point array pattern separated by 200 nm as the ground truth sample (Fig. 2a). This distance is beyond the diffraction-limit resolution of conventional confocal microscope[26, 27]. The ground truth sample is convoluted by nSSM PSF which corresponds to the nSSM imaging process (Fig. 2b, c). In the meanwhile, the image should be processed as follows with the image reconstruction algorithm: i) eliminate the overlaid sidelobes on the image (Fig. 2d, e); ii) correct the image drift relative to each imported image (Fig. 2f); iii) merge the final high spatial frequency image. For these purposes, we coded an automated sub-pixel precision software. In this software, the method of linear deconvolution is used to eliminate the sidelobes and correct the brightness distortion[28]. Then, the method of cross-correlation is used to correct the relative position drift of the image[29] (Supplementary Code). Finally, it is a key step to export the resultant SR image. We reconstructed the image by combining in the spatial domain and frequency domain[30]. In the spatial domain, we extracted the minimum pixel value of two images and obtain image A; in the frequency domain, we extracted the maximum pixel value of two images and obtain image B. The combination of both produced the final SR image. This operation compensated the resolution loss, which was introduced in the step of eliminating the sidelobes by linear deconvolution. We found that only two original images were needed for the reconstruction of nSSM, which thus enables rapid SR imaging in computing resource-limited situations. Compared with the confocal microscope image (Fig. 2g), nSSM improved the resolution to reveal distinctly visible spots (Fig. 2h).

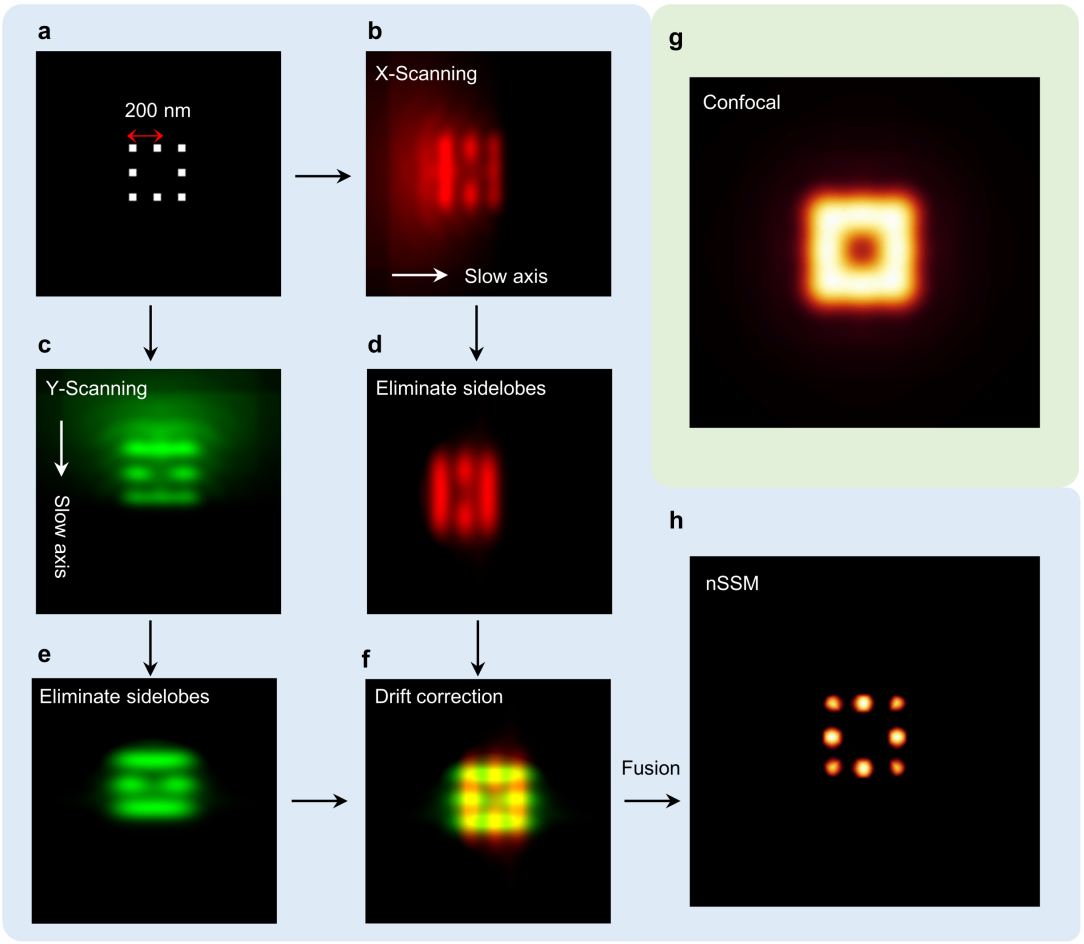

Fig. 2| nSSM image reconstruction work flow with simulated result. a, Ground truth sample with the bright spot separated by the distance of 200 nm. **b**, **c**, Longitudinal (**b**) and horizontal (**c**) scanning image of the sample. **d**, **e**, Images after eliminating the sidelobes and correcting brightness distortion of the longitudinal (**d**) and horizontal (**e**) scanning image. **f**, Overlapped image of (**d**) and (**e**) after drift correction. **g**, Simulated confocal microscope image on sample. **h**, Reconstructed final nSSM image from (**f**).

Experimental determination of the PSF of nSSM. To experimentally determine the PSF of the nSSM system, we employed a designer DNA origami nanostructure that featured an ultra-small (40 nm) fluorescent dye cluster as the fluorescent standard sample (Fig. 3a, b, Supplementary Fig. 2). With the cumulative exposure dose (7 to 192 mJ cm^{-2}), we obtained the nSSM PSF evolution on this standard sample using a commercial confocal microscope. Consistent with the simulation, with the increasing laser exposure dose, the circular PSF squashed as a narrow strip and the sidelobes emerged with the laser dose increase. By overlaying with the same confocal microscope PSF, we found that the nSSM PSF laid on the top of the confocal microscope PSF (Fig. 3c). The aggregated fluorescent DNA origami could be distinguished as two separated spots by nSSM, whereas confocal microscope could not (Supplementary Fig. 3). To quantify the resolution, we measured the FWHM from the mainlobe of the nSSM PSF. When the incident laser exposure dose was 7 mJ cm^{-2}, the confocal microscope worked

in the linear region and the resolution was 275 nm. When the incident laser exposure dose increased to 192 mJ cm^{-2}, the confocal microscope worked in non-linear region and the resolution reached 105 nm (Fig. 3d). The observed FWHM curve manifested the presence of the photon switch-off effect. The consistency in the experimental results, including the PSF form and the resolution trend, with the simulation (Fig. 1d, f) thus substantiated the validity of the nSSM scheme.

To demonstrate the compatibility of nSSM with cell imaging, we carried out nSSM imaging on the immune-labeled cell cytoskeleton structure (Fig. 3e, f). We found that

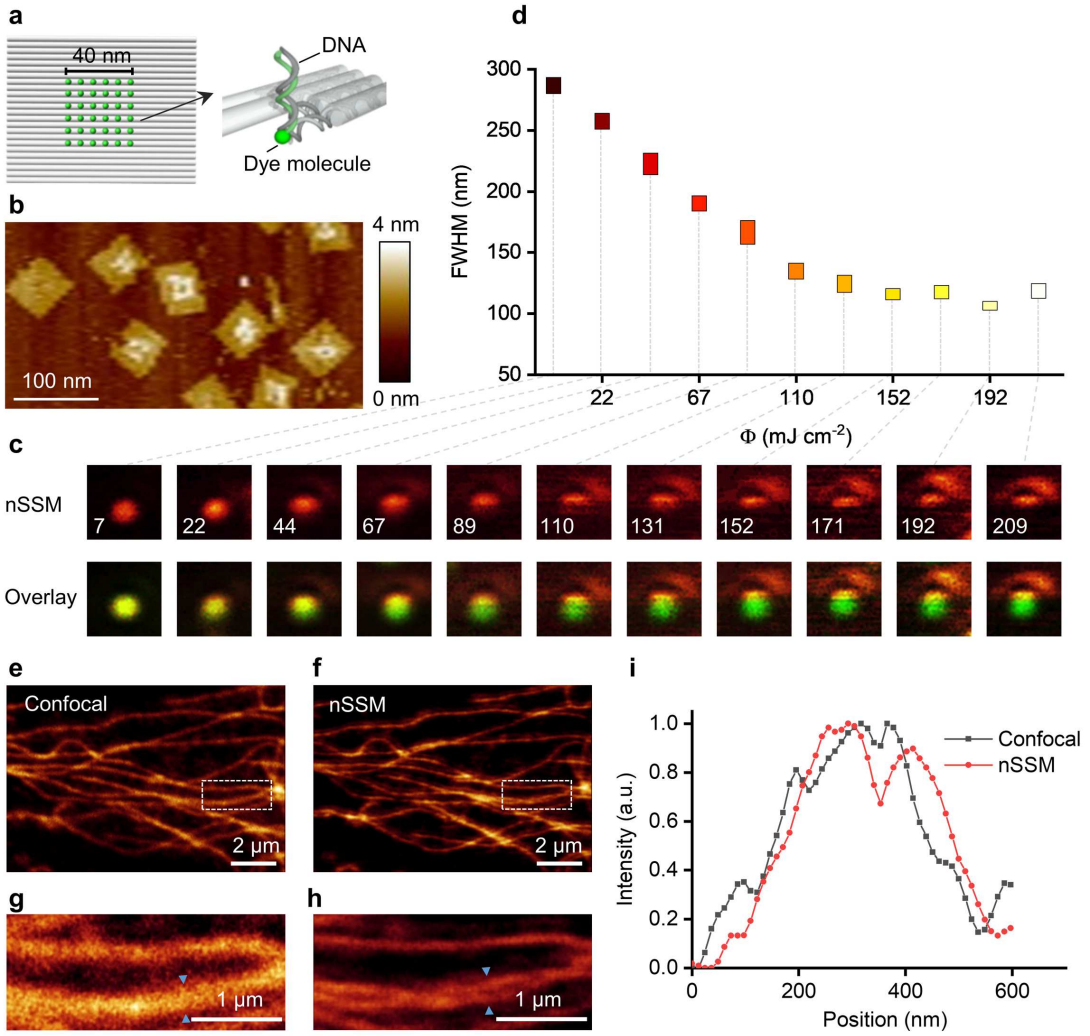

Fig. 3| PSF and resolution measurement on origami standard sample and biological sample. **a**, Standard sample design based on DNA rectangle origami. **b**, Height of the formed fluorescent DNA origami verified by atomic force microscopy in liquid surroundings. **c**, nSSM PSF evolution and overlap image with corresponding confocal microscope PSF with cumulative excitation laser exposure dose for DNA origami imaging. The figures on the corner indicate the exposure does by the unit of mJ cm^{-2}. The size of all images is 1 μm on a side. **d**, Resolution measurement on DNA origami standard sample with cumulative excitation laser exposure dose. **e, f**, Microtubule imaged by confocal microscopy (**e**) and nSSM (**f**). **g, h**, Zoom in from (**e**) and (**f**). **i**, Intensity profile extracts from the double arrow in (**g**) and (**h**) to show the resolution.

the tightly intertwined tubulin fiber observed under the conventional confocal microscope could be distinguished under the nSSM scheme (Fig. 3g, h). The resolution of the nSSM on the organic dye labelled cell reached 100 nm (Fig. 3i). We further demonstrated the generality of the nSSM method by using a range of organic dye, including Alexa 405 and Alexa 488 (Supplementary Fig. 4, Supplementary Fig. 5), which all revealed finer structures in cell imaging.

Live-cell imaging with dronpa. nSSM is intrinsically fast imaging method that is compatible with live-cell imaging as only two frames are needed for all SR direction. To realize live-cell imaging with nSSM, we employed a dronpa fluorescent protein that can be switch on and off repeatedly by the photon controlled conformational transformation[23]. With the wavelength of 488 nm laser incident, dronpa can be switched off and on with a 405 nm laser (Fig. 4a, Supplementary Fig. 6) [31]. We tested the dronpa protein reversible photoswitching characteristics under the illumination of 488 nm laser on a confocal microscope (Fig. 4b). By controlling the laser power and scanning speed, we could finely control the exposure dose of the sample, which thus supports two work modes of nSSM: the high-speed mode with relative high incident power and short pixel dwell time; and the high-resolution mode with relative low incident power and long

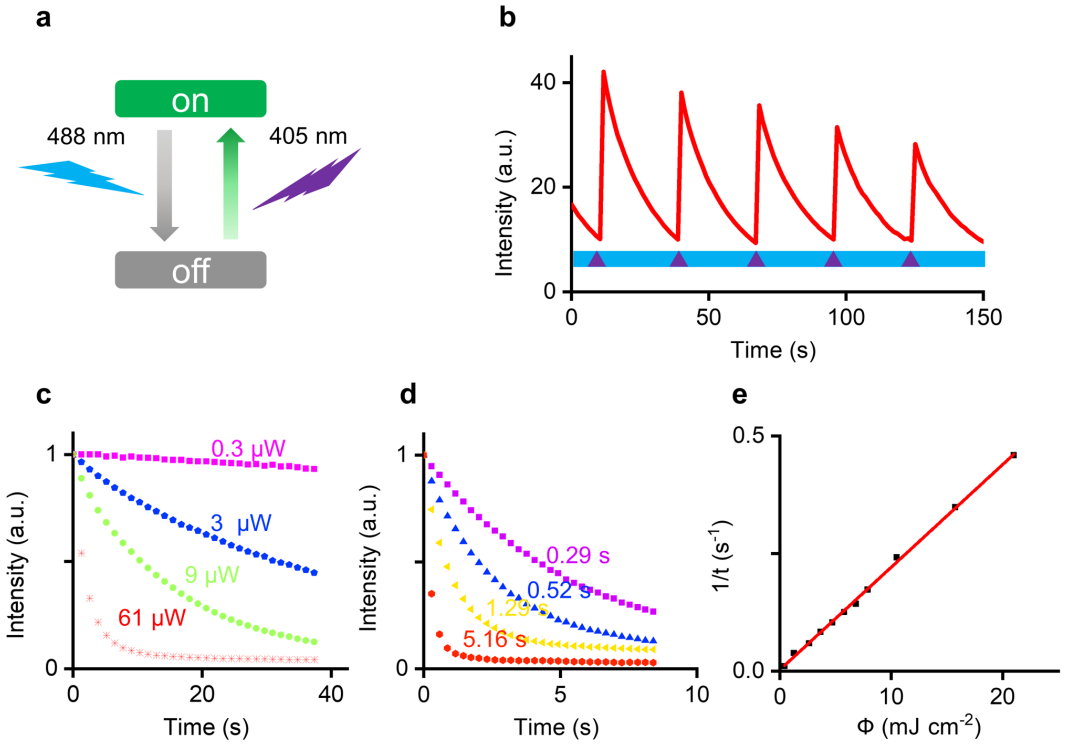

Fig. 4| Properties of dronpa for nSSM. a, Sketch for dronpa switch off and on mechanism. **b**, Intensity trace of dronpa with alternate exposure of switch-off (excitation) and switch-on laser. The blue shadow and the purple arrow indicate the incident laser at the wavelength of 488 nm (9 μW) and 405 nm (72 μW). Irradiation power with 405 nm was chosen so that most of the proteins were switched on. **c, d**, Excitation laser power (**c**) and frame acquisition time (**d**) controlled exposure dose to switch-off the dronpa. **e**, Switch-off rate with cumulative exposure dose.

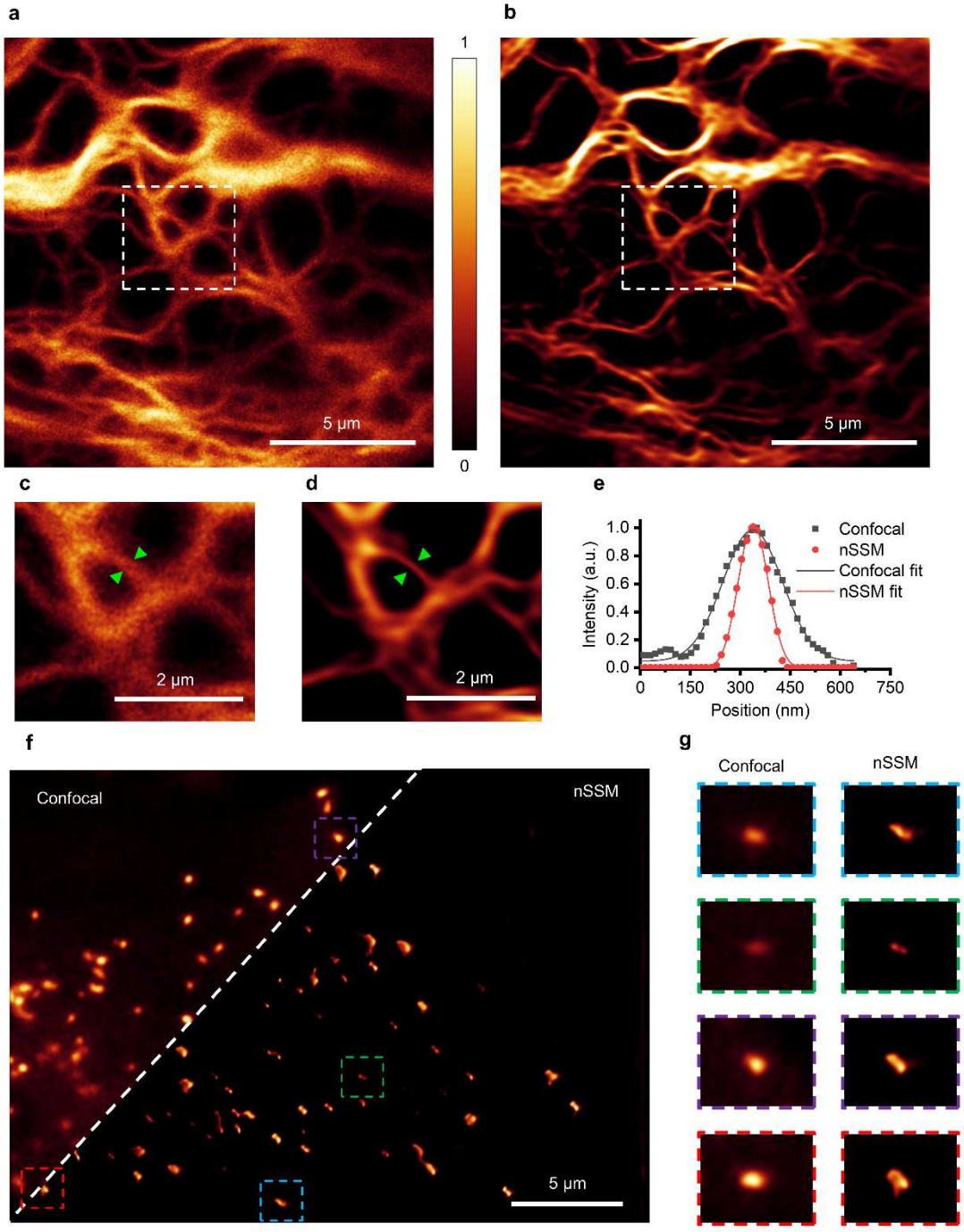

Fig. 5| nSSM imaging of dronpa labelled live cells. a, b, Vimentin imaging by confocal microscope (**a**) and nSSM (**b**). **c, d**, Region of interest of confocal microscope (**c**) and nSSM (**d**) in the white box in **a** and **b**. **e**, Resolution quantification on the intensity profile extracted from the green double arrows. **f**, Peroxisome imaging by confocal microscope and nSSM. **g**, Image performance comparison between confocal microscope and nSSM extracted from the corresponding dash box with different color in **f.**

pixel dwell time. We measured the fluorescence decay curve under the fixed line scanning speed (400 Hz) or fixed incident laser power (4.62 μW, Fig. 4c,d). From these curves, we calculated the incident laser exposure dose and extracted the switch off rate. We found that the switch off rate of dronpa was linearly proportional to the exposure dose of the sample (Fig. 4e).

Next, we determined our nSSM performance on the dronpa labelled vimentin transfected cell. Under the instruction of the nSSM work flow and measured parameter of the dronpa protein, we imaged the vimentin in living Hela cells with a commercial confocal microscope (Fig. 5a). Comparison of the images from the conventional confocal microscope with the nSSM under the laser power of 169 μW and line scanning speed of 10 Hz, we observed the greatly improved resolution for imaging finer cell structures (Fig. 5b). By selecting a representative region of interest (Fig. 5c, d), we measured the FWHM of a single fiber to reveal that the nSSM resolution for live-cell imaging reached 104 nm (vs. 210 nm in conventional imaging) (Fig. 5e). We further realized nSSM imaging of protein structures in dronpa labelled peroxisome cells (Fig. 5f, g).

In summary, by exploiting the omnipresent photon switch-off effect[32], we herein proposed and experimentally demonstrated the nSSM that can in principle be coupled with any commercial confocal microscope. SR images could be reconstructed with a free-code software and limited computing resources. These features of nSSM compare favorably toward affordable SR imaging with stimulated emission depletion (STED) microscopy[33], stochastic optical reconstruction microscopy (STORM)[34] and other SR imaging schemes that rely heavily on hardware or software resource. Compared with structured illumination microscopy (SIM) that is a multi-direction scanning method[35], nSSM is an intrinsically faster imaging method since only two frames are needed for all SR direction. Since the nSSM scheme combines the non-linear switch-off effect and the laser scanning excitation strategy, it may be extended to other excitation laser scanning based microscopy, including spinning disk confocal microscope[36], structured illumination microscope[35], 4Pi[37]. Hence, we envision that nSSM will play as a plug-in to enable multi-wavelength multi-mode living-cell super-resolution imaging on commercial confocal microscopes for widespread use in biological and medical laboratories.

References

1. Sahl, S.J., Hell, S.W. & Jakobs, S. Fluorescence nanoscopy in cell biology. *Nat. Rev. Mol. Cell Biol.* **18**, 685-701 (2017).
2. Sigal Yaron, M., Zhou, R. & Zhuang, X. Visualizing and discovering cellular structures with super-resolution microscopy. *Science* **361**, 880-887 (2018).
3. Schermelleh, L. et al. Super-resolution microscopy demystified. *Nat. Cell Biol.* **21**, 72-84 (2019).
4. Webb, R.H. Confocal optical microscopy. *Rep. Prog. Phys.* **59**, 427-471 (1996).
5. Wu, Y. et al. Multiview confocal super-resolution microscopy. *Nature* **600**, 279-284 (2021).
6. Chen, F., Tillberg, P.W. & Boyden, E.S. Expansion microscopy. *Science* **347**,

543-548 (2015).
7. Denkova, D. et al. 3D sub-diffraction imaging in a conventional confocal configuration by exploiting super-linear emitters. *Nat. Commun.* **10**, 3695 (2019).
8. Lee, C. et al. Giant nonlinear optical responses from photon-avalanching nanoparticles. *Nature* **589**, 230-235 (2021).
9. Cho, S., Humar, M., Martino, N. & Yun, S.H. Laser Particle Stimulated Emission Microscopy. *Phys. Rev. Lett.* **117**, 193902 (2016).
10. Müller, C.B. & Enderlein, J. Image Scanning Microscopy. *Phys. Rev. Lett.* **104**, 198101 (2010).
11. Castello, M. et al. A robust and versatile platform for image scanning microscopy enabling super-resolution FLIM. *Nat. Methods* **16**, 175-178 (2019).
12. Zhao, G. et al. Nonlinear Focal Modulation Microscopy. *Phys. Rev. Lett.* **120**, 193901 (2018).
13. De Luca, G.M.R. et al. Re-scan confocal microscopy: scanning twice for better resolution. *Biomed. Opt. Express* **4**, 2644-2656 (2013).
14. Stennett, E.M.S., Ciuba, M.A. & Levitus, M. Photophysical processes in single molecule organic fluorescent probes. *Chem. Soc. Rev.* **43**, 1057-1075 (2014).
15. Yang, Z. et al. Super-resolution fluorescent materials: an insight into design and bioimaging applications. *Chem. Soc. Rev.* **45**, 4651-4667 (2016).
16. Nienhaus, K. & Ulrich Nienhaus, G. Fluorescent proteins for live-cell imaging with super-resolution. *Chem. Soc. Rev.* **43**, 1088-1106 (2014).
17. Werner, C., Sauer, M. & Geis, C. Super-resolving Microscopy in Neuroscience. *Chem. Rev.* **121**, 11971-12015 (2021).
18. Li, C. et al. Pulsed Saturated Absorption Competition Microscopy on Nonbleaching Nanoparticles. *ACS photon.* **7**, 1788-1798 (2020).
19. Zhao, G. et al. Saturated absorption competition microscopy. *Optica* **4**, 633-636 (2017).
20. Rego, E.H. et al. Nonlinear structured-illumination microscopy with a photoswitchable protein reveals cellular structures at 50-nm resolution. *Proc. Nat. Acad. Sci.* **109**, E135-E143 (2012).
21. Song, L., Hennink, E.J., Young, I.T. & Tanke, H.J. Photobleaching kinetics of fluorescein in quantitative fluorescence microscopy. *Biophys. J* . **68**, 2588-2600 (1995).
22. van de Linde, S. & Sauer, M. How to switch a fluorophore: from undesired blinking to controlled photoswitching. *Chem. Soc. Rev.* **43**, 1076-1087 (2014).
23. Ando, R., Mizuno, H. & Miyawaki, A. Regulated Fast Nucleocytoplasmic Shuttling Observed by Reversible Protein Highlighting. *Science* **306**, 1370-1373 (2004).
24. Warren, M.M. et al. Ground-state proton transfer in the photoswitching reactions of the fluorescent protein Dronpa. *Nat. Commun.* **4**, 1461 (2013).
25. Widengren, J. & Rigler, R. Mechanisms of photobleaching investigated by fluorescence correlation spectroscopy. *Bioimaging* **4**, 149-157 (1996).
26. Willig, K.I., Harke, B., Medda, R. & Hell, S.W. STED microscopy with

continuous wave beams. *Nat. Methods* **4**, 915-918 (2007).
27. Tortarolo, G., Castello, M., Diaspro, A., Koho, S. & Vicidomini, G. Evaluating image resolution in stimulated emission depletion microscopy. *Optica* **5**, 32-35 (2018).
28. Schrader, M., Hell, S.W. & Voort, H.T.M.v.d. Three-dimensional super-resolution with a 4Pi-confocal microscope using image restoration. *J. Appl. Phys.* **84**, 4033-4042 (1998).
29. Tang, Y., Wang, X., Zhang, X., Li, J. & Dai, L. Sub-nanometer drift correction for super-resolution imaging. *Opt. Lett.* **39**, 5685-5688 (2014).
30. Krüger, J.-R., Keller-Findeisen, J., Geisler, C. & Egner, A. Tomographic STED microscopy. *Biomed. Opt. Express* **11**, 3139-3163 (2020).
31. Li, X., Chung, L.W., Mizuno, H., Miyawaki, A. & Morokuma, K. A Theoretical Study on the Nature of On- and Off-States of Reversibly Photoswitching Fluorescent Protein Dronpa: Absorption, Emission, Protonation, and Raman. *J. Phys. Chem. B* **114**, 1114-1126 (2010).
32. Li, H. & Vaughan, J.C. Switchable Fluorophores for Single-Molecule Localization Microscopy. *Chem. Rev.* **118**, 9412-9454 (2018).
33. Vicidomini, G., Bianchini, P. & Diaspro, A. STED super-resolved microscopy. *Nat. Methods* **15**, 173-182 (2018).
34. Rust, M.J., Bates, M. & Zhuang, X. Sub-diffraction-limit imaging by stochastic optical reconstruction microscopy (STORM). *Nat. Methods* **3**, 793-796 (2006).
35. Saxena, M., Eluru, G. & Gorthi, S.S. Structured illumination microscopy. *Adv. Opt. Photonics* **7**, 241-275 (2015).
36. Qin, S., Isbaner, S., Gregor, I. & Enderlein, J. Doubling the resolution of a confocal spinning-disk microscope using image scanning microscopy. *Nat. Protoc.* **16**, 164-181 (2021).
37. Schrader, M., Bahlmann, K., Giese, G. & Hell*, S.W. 4Pi-Confocal Imaging in Fixed Biological Specimens. *Biophys. J* . **75**, 1659-1668 (1998).

Online Methods

Materials. All staple DNA strands for the formation of the origami were purchased from Invitrogen. Alexa-488 functionalized fluorescent DNA strands were purchased from TAKARA. M13mp18 single-stranded DNA was purchased from New England Biolabs. Ultrafiltration device (UFC510096) was purchased from Millipore. Chemicals related to the formation of the DNA origami were purchased from Sinopharm and Sigma-Aldrich. Vimentin dronpa plasmid (57305) and peroxisome dronpa plasmid (54690) were obtained from Addgene. Lipofectamine 3000 transfection reagent (L3000008) and opti-MEM (31985062) were purchased from Thermo Fisher Scientific. Triton X-100 (93443) and paraformaldehyde (158127) were purchased from Sigma-Aldrich. Normal goat serum (NGS, ab7481) and aqueous mounting medium (F4680) obtained from Sigma-Aldrich. Glass slides and coverslips were purchased from Corning. Living cell culture dish (D35-14-1.5-N) was purchased from Cellvis. Primary antibody (ab6160) and organic dye labeled antibody, including Cy3 (ab6953), Alexa 488 (ab150157), were purchased from Abcam. Dylight 405 labelled secondary antibody (A23140) was purchased from Abbkine. All materials were used for experiment without further purification.

Photon switch-off model. The photon physical model of the probe with bright and dark state can be modelled as Jablonski energy level diagram showen in Fig. 1a. In this model, bright state simplified as ground state (B) and excitated state (B*), dark state simplified as one non-fluorescence state (D). The probe at ground state absorbe a incident photon and then transites to excited state. The electron at excited level emitted a photon or transites to dark state. A part of probe in dark state will stay in dark state permanently and some of probe will return to bright state spontaneously or exposure by a special laser, like 405 nm.

The population probability of the levels of the probe with rate equation shows as:

$$\frac{dN_B}{dt} = -k_{exc}N_B + k_f N_{B^*} + k_{on}N_D$$

$$\frac{dN_{B^*}}{dt} = k_{exc}N_B - (k_f + k_{off})N_{B^*}$$

$$\frac{dN_D}{dt} = k_{off}N_{B^*} - k_{on}N_D$$

In this rate equation, the N_B, N_{B^*}, N_D donate the population of the fluorescent probe at ground state, excitation state and dark state, respectively. k_{exc} and k_f donate the excitation and fluorescence transit rates, respectively. k_{on}, k_{off} donate the transition rate of $D \to B$, $B^* \to D$, respectively. $k_{exc} = \sigma I_{exc}\lambda/\mathrm{hc}$, with the probe absorption cross section $\sigma = 10^{-17}$ cm^{-2}, incident laser power density I_{exc}, incident light wavelength λ= 488 nm, Planck constant h and speed of light c.

The excitation laser spot of confocal microscope was calculated by using of vectorial diffraction theory for the high numerical aperture objective[38]. The numerical aperture, wavelength of the excitation laser and refractive index of imaging were taken to be 1.4, 488 nm and 1.518. The nSSM effective point spread function (PSF) was calculated by coupled rate equations. The fluorescence signal intensity was characterized by the molecular population at the bright state. The resolution was represented by FWHM of

the mainlobe. The exposure dose was controlled by the pixel dwell time and excitation rate.

Image reconstruction algorithm. Image A (I_A) and image B (I_B) with orthogonal scanning direction were pre-processed by Leica LAS X software. The image reconstruction algorithm was codded by MATLAB. To obtain sub-pixel high-precision reconstructed image, the experiment images were up-sampled 2× by bicubic interpolation. The sidelobes were eliminated by linear deconvolution. The linear deconvolution PSFs were constructed by simulation or experiment results. We split the ideal nSSM effective PSF as sidelobes function (artifact, $h_{side}(\boldsymbol{r})$) and mainlobe function (signal, $h_{main}(\boldsymbol{r})$). The linear deconvolution PSF was the summation of weighted distributions (δ) of the mainlobe function and sidelobe function.

$$h_{lin}(\boldsymbol{r}) = h_{main}(\boldsymbol{r}) + \delta h_{side}(\boldsymbol{r}) \quad (-1 < \delta < 0)$$

The weight of the mainlobe function is positive, whereas sidelobe function is negative. We carried out convolution operation on the linear deconvolution PSF and the image.

$$I_A' = I_A \otimes h_{lin}(\boldsymbol{r})$$

The drift correction of the sidelobe eliminated images could be carried complete automated with the cross-correlation algorithm[29]. The drift correction images were merged twice by extracting the minimum value in spatial domain, and maximum value in Fourier domain.

$$\mathrm{I} = \mathrm{argmin}(I_A, I_B) * \mathcal{F}^{-1}(\mathrm{argmax}(\mathcal{F}(I_A), \mathcal{F}(I_B)))$$

$\mathcal{F}$ and $\mathcal{F}^{-1}$ donate the Fourier transform and inverse Fourier transform, respectively. The final image was merged by the product of the obtained two images and the deteriorated image resolution caused by the sidelobe eliminated process could be recovered.

Optical set-up. All optical measurements were carried out on a commercial confocal microscope (Leica TCS-SP8, Germany) equipped with a 63×/1.4 objective and a HyD detector. The sample were excited by the laser at the wavelength of 405 nm emission from a diode laser or 488 nm emission from an argon-ion laser. Dronpa protein was photo-actived by the laser at the wavelength of 405 nm. The pixel size and the pinhole are set to 6-12 nm and 286.6 μm, respectively. The exposure dose was controlled by the incident laser power and the scanning speed, meanwhile, the fluorescence signal was recorded by HyD detector. The exposure does (Φ) of the sample is calculated by

$$\Phi = \mathrm{Pt/S}$$

Where P is the power of the incident laser measured at the rear focal plane of the objective, t is the acquire time of the image and S is the area of the image region.

DNA origami standard sample. The rectangle DNA origami were formed in a one-pot reaction with a 100 μl total volume containing 500 nM scaffold strand[39]. The extruding strands of DNA single strand on DNA origami was replaced by customized DNA single strand (5'→3' staple-AAAAAACAGGACCAGAAAAAA) (Supplementary Table). Then, the purified DNA rectangle origami were mixed in a 1:10 concentration ratio with the complementary single-stand fluorescent DNA (5'→3' TTTTTTCTGGTCCTGTTTTTT-Alexa Fluor 488) and annealed from 45° to 15°C at a

speed of 0.1 °C/min. The obtained DNA origami standard sample was cleaned four times by ultrafiltration device. The morphology of the DNA origami was characterized by atom force microscope in liquid environment after monodispersing on the surface of mica. DNA origami standard sample mixed with the aqueous mounting medium with the ratio of 1:2 and sandwiched into the middle of the cover slip and slide for confocal microscope measurement.

Cell sample. Hela cells were cultured in high glucose MEM medium supplemented with 1% penicillin/streptomycin, 10% (v/v) fetal bovine serum, 2 mM L-glutamine and maintained in humidified air containing 5% CO_2 at 37 °C.

For dronpa protein fluorescence imaging sample, the cell suspension was seeded into sterile 35-mm glass-bottomed cell culture dishes at a density of 10^5 cells per dish and incubated for 24 hours to allow cell adherence. 1 ug vimentin or peroxisome dronpa plasmid were transduced into cells by Lipofectamine 3000 transfection reagent with the instructions from the manufacturer. After 24 h transfection, cells were washed by phosphate-buffered saline (PBS) solution and fixed with 4% (w/v) paraformaldehyde (PFA) solution for nSSM imaging.

For the microtubule immunostaining sample, the monodispersed HeLa cells were cultivated on 12 well cell culture plate with pre-placed coverslips. The cells were washed once in pre-warmed PBS, fixed by application of pre-warmed PFA fixation buffer for 15 min and permeabilized with 0.2% (w/v) Triton X-100 in PBS for 15 min. Fixed and permeabilized cells were blocked with block buffer (10% normal goat serum (NGS), 0.05% Triton X-100 in 1× PBS) for 60 min and were incubated with primary anti-tubulin antibody (dilute with 1:200) in antibody incubation buffer (AIB) for 60 min (AIB: 5% NGS and 0.05% Triton X-100 in 1× PBS). After removing the superfluous primary anti-tubulin antibody by washing with AIB, the cells were followed incubated with fluorescent dye (Alexa Fluor 405, Atto 488, Cy3) labeled secondary antibody (dilute with 1:200) for 60 min. Cells were again washed three times for 10 min each with AIB and then were optionally post-fixed by incubating with 4% PFA in 1× PBS for 15 min. The coverslip with cells were glued to a microscope slide by aqueous mounting medium. All experiments were performed at room temperature. Except for the fix and post-fix step, all experiments were performed while shaking.

References

38. Gao, Z. et al. Spaser Nanoparticles for Ultranarrow Bandwidth STED Super-Resolution Imaging. *Adv. Mater.* **32**, 1907233 (2020).
39. Fang, W. et al. Quantizing single-molecule surface-enhanced Raman scattering with DNA origami metamolecules. *Sci. Adv.* **5**, eaau4506 (2019).

Acknowledgments

This work was supported by the National Key R&D Program of China (2020YFA0908900), the National Natural Science Foundation of China (22104089, 62065012, 61665006, 21834007, T2188102), the Interdisciplinary Innovation Fund of Natural Science, Nanchang University (No. 9167-28220007-YB2111), the Science Foundation of Shanghai Municipal Science and Technology Commission (21YF1420700, 19JC1410300).

Author contribution

C.F., H.-Y.C. and B.K. conceived and supervised the study. Z.G., S.H. and S.D. designed and performed experiments and carried out the simulation. Z.G. designed and coded the super-resolution image reconstruction program. Z.G., S.H. and S.D. analysed the data and wrote the initial manuscript. All authors discussed the results and commented on the manuscript.

Competing financial interests

The authors declare no competing financial interests.

Supplementary Files

This is a list of supplementary files associated with this preprint. Click to download.

- SupplementaryCode.zip
- NonlinearscanningswitchoffmicroscopySupplementaryInformation.docx
- nSSMPSFwithcumulativelaserpower.avi